ELSEVIER

Polymer 42 (2001) 9015–9023

polymer

www.elsevier.com/locate/polymer

Time-resolved shear behavior of end-tethered Nylon 6–clay nanocomposites followed by non-isothermal crystallization

Francisco J. Medellin-Rodriguez[a], Christian Burger[a], Benjamin S. Hsiao[a], Benjamin Chu[a,*], Richard Vaia[b], Shawn Phillips[c]

[a]*Department of Chemistry, State University of New York at Stony Brook, Stony Brook, NY 11794-3400, USA*
[b]*Air Force Research Laboratory, AFRL/MLBP, 2941 P St., Wright-Patterson AFB, OH 45433-7750, USA*
[c]*Air Force Research Lab, 10 E. Saturn Blvd., Bldg. 8451 Edwards AFB, CA 93524-7680, USA*

This work is devoted to Prof. Stein on the occasion of his 75th Birthday

Received 9 March 2001; accepted 26 March 2001

Abstract

Simple shear of end-tethered Nylon 6–clay nanocomposites and the preservation of these effects into the crystalline state is reported. Typical conditions leading to mesoscopic (clays) and molecular (polymer chains) orientation of these systems at relatively low shear rates and at temperatures immediately above the nominal melting point showed a morphological change proportional to the shear time in the molten state. Gradual alignment of the through-view SAXS patterns indicated the rotation of the end-tethered clay along the shear direction. High temperature relaxation of clay after shear was substantially longer than the polymer. Thus, non-isothermal crystallization into the crystalline state could be used to preserve the orientation of the clay induced by shear. It was found that most of the clay planar alignment in Nylon 6–clay nanocomposites rendered the γ crystal habit, which is typically associated with the extended chain crystallization. Nylon 6, on the other hand, crystallized into the α habit commonly associated with quiescent crystals involving folded chains. The shear results were compared with quiescent crystallization, where the Nylon 6 nanocomposites exhibited the preferential γ habit and the Nylon 6 homopolymer exhibited mixed α/γ habits.

Keywords: Polymer nanocomposites; Nylon 6; Clay

1. Introduction

In contrast to the filled or fiber-reinforced polymer systems, several new thermoplastic nanocomposites have recently been developed. One notable example is Nylon 6–clay hybrids (NCH), which can be identified by its intimate polymer particulate interactions. There is evidence that a major fraction of the clay particles has been 'exfoliated' in NCH. The exfoliation in this system was achieved through high temperature ring-opening polymerization of ε-caprolactams, which became tethered to the clay surface [1–3]. NCH are among the most practical nanocomposite polymeric systems because they can be processed in the molten state by injection molding or extrusion. The injection-molded articles have displayed improved tensile and flexural strength and modulus [4], heat distortion temperature [5] and gas barrier properties [6], together with a lower erosion rate [7] and higher resistance to permeation [8] than unfilled Nylon 6.

The objective of this study is to understand the role of exfoliated clay particles on the molecular orientation of the Nylon chains and the post effects on the crystal structure and morphology by processing such as shear.

Oscillatory shear with small strain amplitudes of Nylon 6 nanocomposites has been reported by Krishnamoorti and Giannelis [9]. As in conventional filled systems, it was found that the storage and loss moduli increased with increasing clay loading except in the terminal zone. In terms of structure and morphology, Kojima et al. [10,11] studied the crystallized NCH in thin films and solid injection-molded bars. X-ray diffraction results indicated that the clay particles induced preferred orientation of the Nylon 6 crystallites and that the degree of orientation of crystallites increased with the clay content.

In terms of the crystal structure of Nylon 6, Brill [12] and Holmes et al. [13] determined the α-form in the fiber specimen. This form consists of a monoclinic unit cell ($a = 9.56$ Å, $b = 17.24$ Å, $c = 8.01$ Å, $\beta = 67.5°$) with the b

* Corresponding author.
E-mail address: bchu@notes.cc.sunysb.edu (B. Chu).

0032-3861/01/$ - see front matter
PII: S0032-3861(01)00395-0

dimension being along the fiber axis. There are eight monomeric units in the unit cell with extended-chain sheet structure and hydrogen bonding between the anti-parallel chains. Such an arrangement can be achieved by adjacent re-entry of the folded chains, as in quiescent crystallization. Holmes et al. [13] and Arimoto et al. [14] also determined the γ-form of Nylon 6, consisting of a monoclinic unit cell ($a = 9.33$ Å, $b = 16.88$ Å, $c = 4.78$ Å, $\beta = 121°$) with the b dimension being along the fiber axis. This form has four monomeric units in the unit cell and hydrogen bonding between parallel chains. The γ-form is often associated with the formation of extended chain crystals and is typically obtained from processing involving elongational flow, such as in fiber spinning [15].

It is important to understand the morphological evolution of NCH in the molten and crystalline states during processing. Such knowledge will be useful to control the properties of the hybrid nanocomposite. For this study, we have explored the effects of simple shear that express aspects of the injection molding process.

2. Experimental

Nylon 6 homopolymer and hybrid nanocomposites containing 2 and 5 wt% of clays were synthesized by polymerization of ε-caprolactam in the presence of organically modified montmorillonite [16] by Ube Industries, Japan. The modified montmorillonite was prepared by a cation exchange reaction with 12-aminolauric acid. The montmorillonite ε-caprolactam chemical reaction rendered poly(caprolactam) chains end-tethered through the 12-aminolauric acid to the silicate surface [17]. Nylon 6 homopolymer (having a weight-average-molecular weight of 2.17×10^4 g/mol) was processed into stretched films using a DACA MicroCompounder. Hybrid nanocomposite films containing 2 wt% (NCH2) and 5 wt% (NCH5) had a weight-average molecular weight of 2.22×10^4 and 1.97×10^4 g/mol, respectively [9]. The films (250 μm thick) were layered and melted at 260°C (held for 5 min) under 1 metric ton of pressure using a Carver high temperature press. Samples were cooled at an average rate of 50°C/min and uniform films with an average thickness of 700 μm were obtained. Ring shape samples with an external diameter of 1 cm and an internal diameter of 0.5 cm were then stamped from these films for shear experiments.

A Linkam CSS-450 high-temperature shearing stage, modified for X-ray diffraction and scattering experiments, was used to control shear flow and to introduce a controlled thermal history to the sample. Two parallel plates were used to sandwich the ring-shaped specimen, and Kapton® films were used in place of the quartz optical windows on the top and bottom steel plates to support the specimen. The top plate had a narrow aperture hole (3 mm in diameter), which allowed the X-ray beam (0.3 mm diameter) to enter the sample. The bottom rotating plate had open slots (wider than the hole in the top window) for the exit X-ray beams. The sample was sheared by rotating the bottom plate through a precision stepping motor while the top plate remained stationary. The bottom opened slots allowed the scattered X-ray beam to be detected during shear. SAXS/WAXD signals were separately measured during shear under identical experimental conditions.

A Perkin–Elmer 7 differential scanning calorimeter (DSC) was used to obtain the thermal behavior of traces of samples before and after shearing experiments. In DSC, samples with an average weight of 8 mg were linearly heated, between 25 and 250°C, at 10°C/min from room temperature in the presence of nitrogen.

Transmission electron microscopy (TEM) images were obtained using a JEOL 1200EX microscope with an accelerating voltage of 80 kV. A piece of the sample in film form was end cross sectioned using an American Optical Ultracut microtome, and TEM images were taken along the cross sectioned samples.

SAXS/WAXD measurements were carried out at the Advanced Polymers Beamline (X27C, operating at a wavelength of 1.307 Å) in the National Synchrotron Light Source (NSLS), Brookhaven National Laboratory (BNL). A three-pinhole collimator system was used for beam alignment. A 2D MAR CCD X-ray detector (MARUSA) was employed for the detection of 2D SAXS images, having a resolution of 512×512 pixels (pixel size = 257.6 μm). The sample to detector distance for SAXS was 1270 mm, and for WAXD was 140 mm. The scattering angle of the SAXS pattern was calibrated with the silver behnate, and that of the WAXD profile was calibrated with a silicon standard.

3. Results and discussion

3.1. Melting behavior

Differential scanning calorimetry (DSC) heating scans of as-received, as-prepared, and after-sheared samples of Nylon 6 and NCH5, are shown in Figs. 1 and 2, respectively. Even though the primary purpose of this study was not to rationalize the melting behavior of Nylon 6 hybrids in regards to the neat resin, these features are reflective from the different thermal histories and the shearing conditions. The as-received Nylon 6 and NCH5 samples display a broad melting endotherm, which is more pronounced in NCH5 than Nylon 6, before the crystallization exotherm. The endotherm may be related to the original film casting process since it disappears in the as-prepared samples. The crystallization exotherm following the endotherm can be associated with recrystallization during heating, such as in the system of PEN [18]. The DSC scan of Nylon 6 exhibited a single melting endotherm at 220°C. However, NCH5 displays up to three melting endotherms over a broad range of temperatures. In the latter case, the first two melting endotherms in NCH5 are commonly observed in Nylon

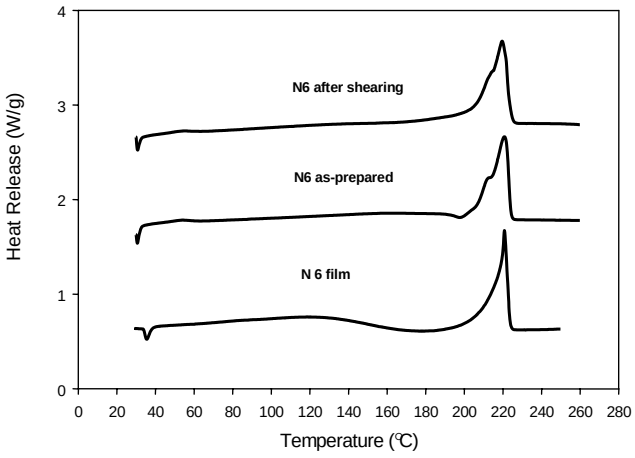

Fig. 1. DSC heating scans of Nylon 6 with different thermal and shear histories. Sample characteristics are shown.

6 homopolymer and have received different explanations [19,20] and the last small melting endotherm is similar to the one observed during crystallization under pressure [21]. The as-prepared and after-sheared samples exhibited a similar melting behavior, consisting of double (Nylon 6) and triple (NCH5) melting endotherms, respectively. It is interesting to note that the final melting temperature did not change in both systems. As the molecular weights of all our samples (Nylon 6 and NCH5) were similar, the effect of molecular weight on the structure change in shear was probably negligible.

As mentioned earlier, Kojima et al. [10,11] studied the orientation of montmorillonite and Nylon 6 crystallites with 60 μm films and 3 mm bars using WAXD. The diffraction characteristics along the face-on in the first case indicated that the polymer molecular axis was randomly oriented on the film plane. Edge and end-view patterns displayed an equatorial diffuse streak at low diffraction angles, which indicated preferred planar orientation of the clay platelets. The meridional orientation of the (002) reflection suggested that Nylon 6 crystallites also assumed a planar orientation along the film plane. Here and below, we are using the terms 'equatorial' and 'meridional' for the directions in shear flow and perpendicular to it, respectively. Strictly speaking, this is not quite valid, as it implies a cylindrical symmetry about an axis in the direction of shear flow that is not present. It is understood that we are using this terminology here only because it is customary and convenient for 2D scattering patterns.

In the present study, simultaneous SAXS/WAXD images were obtained in the as-received and as-prepared films. In agreement with the studies by Kojima et al. [10,11], the as-received NCH films (250 μm thick in average) displayed a random γ-form in through-view WAXD, as shown in Fig. 3. The edge-view pattern, on the other hand, was also in agreement with Kojima et al.'s results. The equatorial clay-related streak and the oriented Nylon 6 crystallite reflections were observed. The corresponding through-view SAXS patterns of the as-received specimens are shown in Fig. 4. In contrast to the narrow streak observed in WAXD, a more diffuse equatorial streak is observed in SAXS. This diffuse equatorial streak [22,23] suggests that a fraction of the clay layers is not oriented parallel but perpendicular to the film plane and aligned relative to the film drawing direction. This observation could be supported by the results from transmission electron microscopy of the sectioned as-received film, as shown in Fig. 5. Clay layers are observed perpendicular to the film plane (see arrows). These give rise to the diffuse meridional intensity in SAXS. We note that a weak scattering maximum is seen in both SAXS patterns, which can be attributed to the crystal lamellar structure. The observed diffuse SAXS profile near the origin is mainly

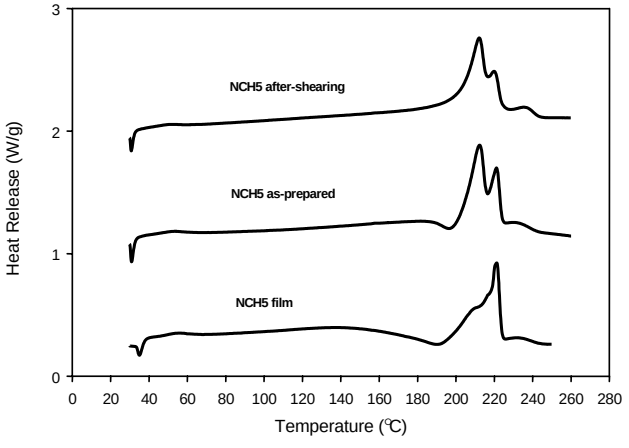

Fig. 2. DSC heating traces of NCH5 with different thermal and shear histories.

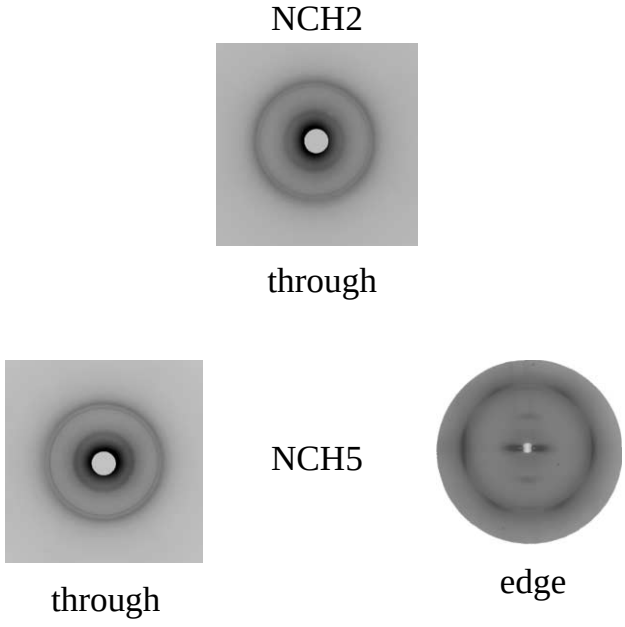

Fig. 3. WAXD patterns of as-received nylon–clay nanocomposite films observed along the through and edge-views as indicated.

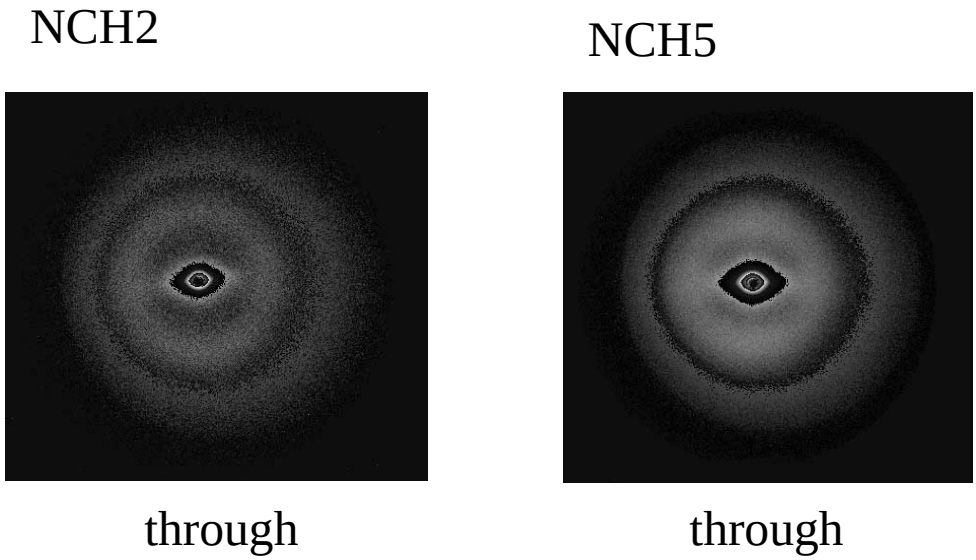

Fig. 4. SAXS patterns of as-received nylon–clay films along the through-view.

due to the scattering from a small fraction of intercalated clays (as in TEM). We believe that the majority of clays is exfoliated generating little scattering intensity to the observed SAXS image.

3.2. Constant rate shearing of nanocomposites

Injection molding operations usually involve shearing processes from the extrusion screw to the die exit and then to the mold chamber. This is usually made at high shear rates between 100 and 200 s^{-1}. To begin to understand the morphological development in this situation, a shear rate of 60 s^{-1} and a total shear time of 20 min were examined. During this process, the fluid elements rotate as well as undergo shearing. The experimental device having a parallel-plate shearing geometry should render a constant shear rate and a constant strain across the thickness of the sample under the ideal steady state condition. However, at the shear rate examined, some tumbling motion (vorticity) is expected. As the dimension of the clay particle is much larger than the polymer chain and the modulus of the clay is much higher, it is reasonable to expect that the

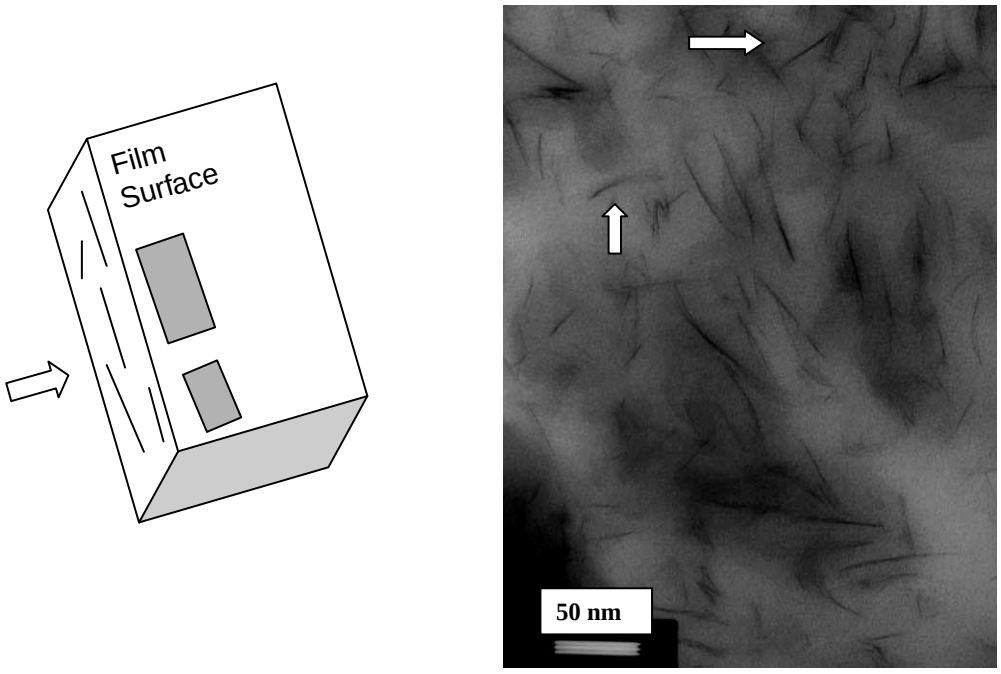

Fig. 5. Bright field TEM image near center of NCH5 as-received film. The film-crossed section is indicated and the clay positional orientations are enhanced. Film surface is parallel to the vertical edge of the micrograph.

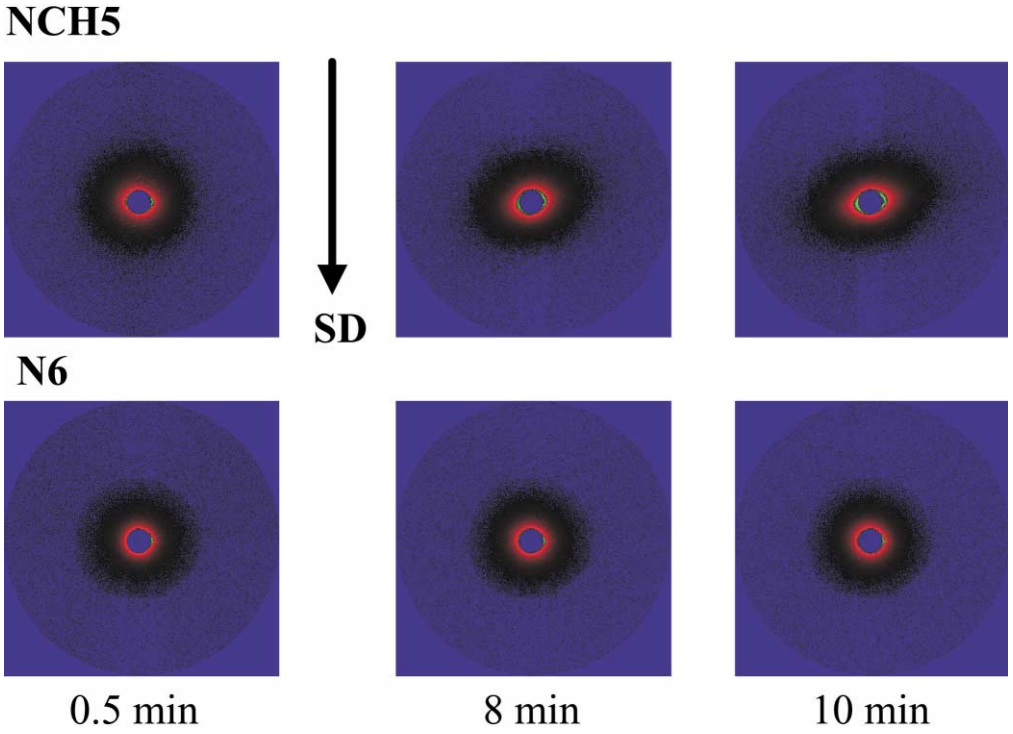

Fig. 6. SAXS patterns of NCH5 and Nylon 6 under shearing ($\gamma = 60\ s^{-1}$; $T = 240°C$) (through orientation). The shearing direction and shear time are shown.

clay particles in nanocomposite are more subject to the tumbling motion during shear than the pure resin.

Typical in situ SAXS patterns of NCH5 above the nominal melting temperature of the neat Nylon 6 resin during constant-rate shear are shown in Fig. 6, where the shear direction is also indicated. The main feature of these patterns is that there is the progressive formation of an oriented scattering pattern (along the equatorial direction) with increasing shearing time. The origin of this pattern can be understood by considering the direction of shear and by noting a fraction of the polymer chains are associated chemically or hydrogen bonded to the clay surface. As a consequence of shear, the stretched absorbed polymer chains may remain oriented (because of the increase in its relaxation time) and the clay plates can be rotated as a result of shear-induced vorticity and the chain orientation. As the temperature was above the nominal melting point of Nylon 6, no scattering associated with Nylon 6 crystallites was observed. The corresponding experiments with Nylon 6 are also shown in Fig. 6 and do not show any orientated features.

Fig. 7 describes the nanocomposite behavior in more detail. Fig. 7a shows the as-prepared samples before shearing where there is overall random orientation of both clay platelets and polymer chains, all giving rise to an isotropic pattern. (Note the small orientation in Fig. 4 is due to the film stretching process.) With increasing shearing time, as shown in Fig. 7b, reorientation of clay platelets takes place due to vorticity produced by the shearing process and the stretching of the absorbed chains to the clay sheets. The observed scattering anisotropy represents only a fraction of the clay platelets that are 'visible' to SAXS during shear. We find that the presence of orientation in the SAXS patterns was progressive with shearing time and that the total scattered intensity (proportional to the clay orientation becoming detectable by SAXS) reached a plateau value after 15 min of shearing, as shown in Fig. 8. This implies that the degree of the clay orientation is increased with both shear time (strain) and the clay content.

A quantitative evaluation of the SAXS data is currently underway, but it will require experimental data with high statistical accuracy. There are two limiting cases, which can serve as a starting point for the quantitative evaluation of anisotropic 2D SAXS data from sheared systems: (1) The anisotropy could be described as purely an orientational effect, or (2) it could be described as a deformation.

In the purely orientational description, an ensemble of structural units (in the present case the clay platelets) with various orientations is averaged over an orientation distribution that is a function of the three Euler angles. In the general case, this leads to fairly involved calculations ('texture analysis"), but certain special cases like cylindrical symmetry of the structural unit and/or of the ensemble can lead to simplifications, which are more tractable ('fiber symmetry'). However, the present experimental geometry cannot be described in terms of the simplest case.

The concept of introducing the anisotropy by a deformation is very appealing because, assuming that the deformation can be formulated as an affine transformation, the resulting effect on the scattering pattern can be simply formulated in

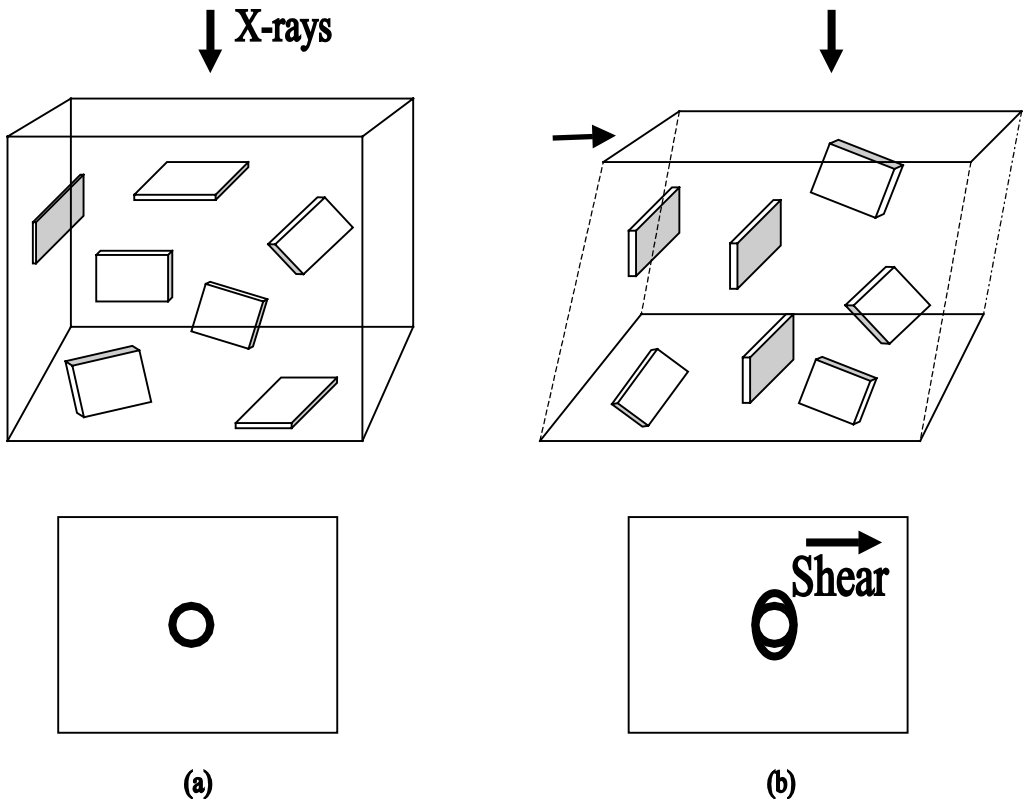

Fig. 7. Representation of clay reorientation through vorticity on shear: (a) before shear; (b) during shear (note that the absorbed polymer chains are aligned with the shear direction, which are not shown).

terms of a 3D generalization of the dilation theorem of the Fourier transformation, $\Im f(\mathrm{Tr}) = |\mathbf{T}|^{-1}(\Im f)(\mathbf{T}^{-1}\mathbf{q})$, where $\mathbf{q}$ is the scattering momentum vector and $\mathbf{T}$ a tensor describing the affine deformation which could, e.g. be a stretching operation along an axis or, more closely related to the present experimental case, a shearing operation transforming a cube into a parallelepiped with oblique angles.

It is not a priori clear which of these two cases is better suited to model the experimental data, but even if the deformation case is not the appropriate one, it should be investigated if it can be used as an approximation, since it is much easier to implement.

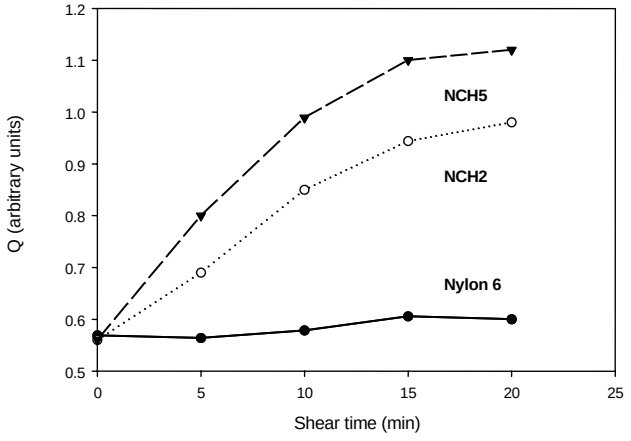

Fig. 8. Total scattering intensity as a function of shearing time.

3.3. Orientation relaxation and non-isothermal crystallization

The preservation of the clay orientation, upon the cessation of shear, was also studied in this work. This effect is similar to the conditions encountered during typical injection molding operations, where the molten polymer is first sheared and then allowed to relax before the crystallization process occurs. The relaxation process is very important in fabricating polymeric materials where highly oriented products are required. A prolonged relaxation process can increase the available operational time to manipulate the anisotropy of the system. Typical time-resolved SAXS patterns during the relaxation process, after 10 min of steady-shear at a shear rate of 60 s^{-1} and 240°C, are shown in Fig. 9. It is seen that the complete relaxation time for de-orientation of the clay platelets, as induced by shear, is around 12 min. Since polymer chains are absorbed onto the clay surface, the disorientation of the clay indicates that a fraction of polymer chains may also have extended relaxation time.

The state of orientation of both polymer chains and nanoclays after shearing can be preserved by non-isothermal

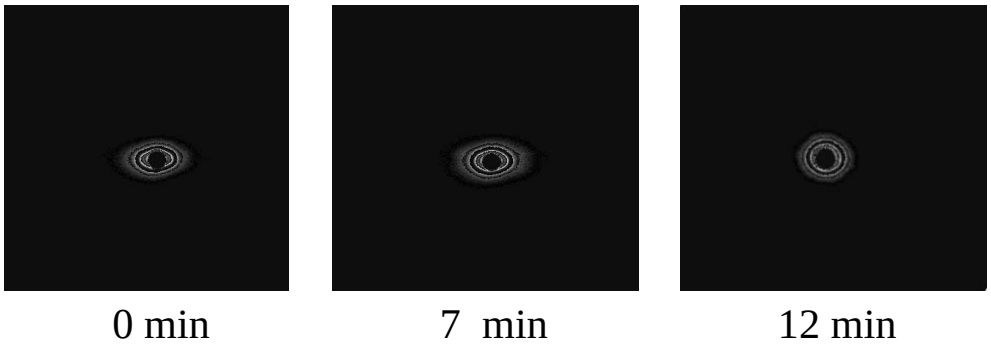

Fig. 9. SAXS relaxation patterns after shear ($\gamma = 60\ s^{-1}$; $T = 240°C$; 10 min). Relaxation times are shown.

crystallization. This is important since the ultimate mechanical properties of the crystallized system can be manipulated. Fig. 10 shows the in situ SAXS pattern during non-isothermal crystallization of NCH5 and Nylon 6. It is observed that the orientation of the clay can be largely retained by non-isothermal crystallization. Without the presence of the clay, the polymer chains cannot be quenched into an oriented state at the chosen shear condition, producing randomly oriented crystallites. The addition of exfoliated clay thus opens up new possibilities of producing better-oriented products by injection molding. It is conceivable that high molecular orientation can also be obtained in the core part of the injection molded NCH nanocomposite. In Fig. 10, it is interesting to note that Nylon 6 displays the typical discrete scattering pattern associated with completely random lamellar structures.

Fig. 11 shows the corresponding WAXD patterns of NCH5 (a) and Nylon 6 (b). In this figure, it is observed that NCH5 exhibits the γ crystal habit under non-isothermal crystallization conditions. As indicated earlier, the γ crystal habit is a characteristic of the oriented morphologies consisting of extended chain crystals [15]. Also, it can be obtained at a high degree of supercooling (i.e. thermally impeded conditions) [19]. At this point, the question at hand is whether the γ-form is induced by the presence of exfoliated clay, the imposed shear condition, the imposed thermal condition or a combination of these factors. To resolve this question, we have carried out the following experiments. Fig. 12 shows the WAXD behavior of quiescent non-isothermal crystallization of both Nylon 6 and NCH5, i.e. without shear. It is evident that in unfilled

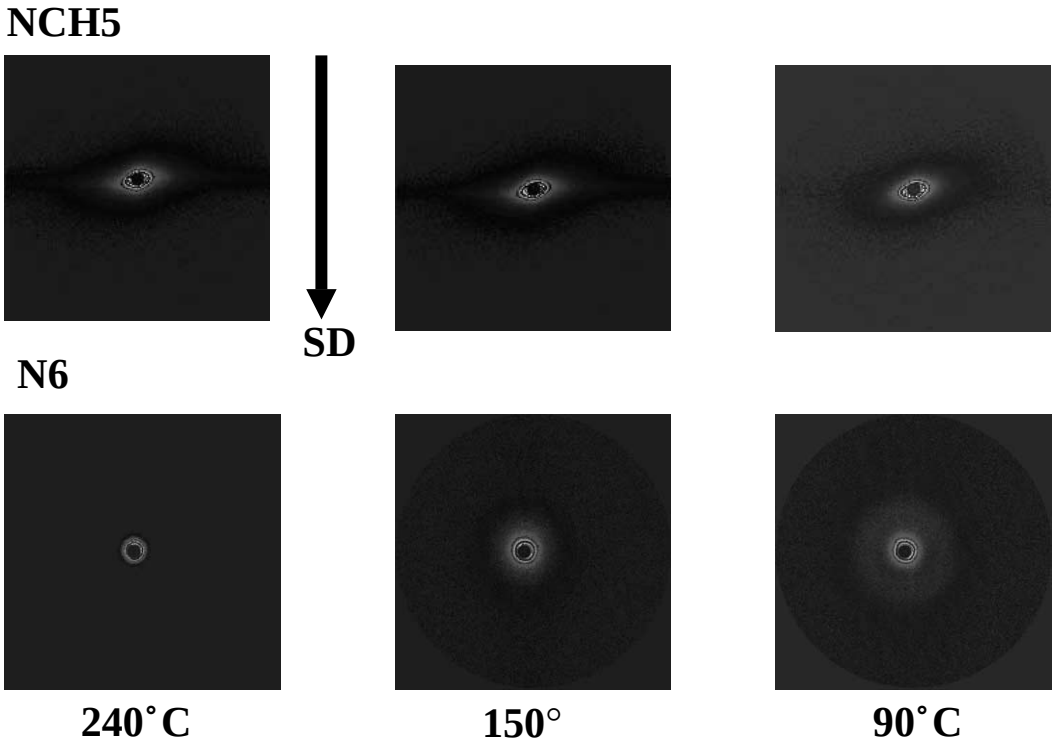

Fig. 10. SAXS patterns under non-isothermal crystallization. The shearing direction is indicated together with specific non-isothermal crystallization temperatures.

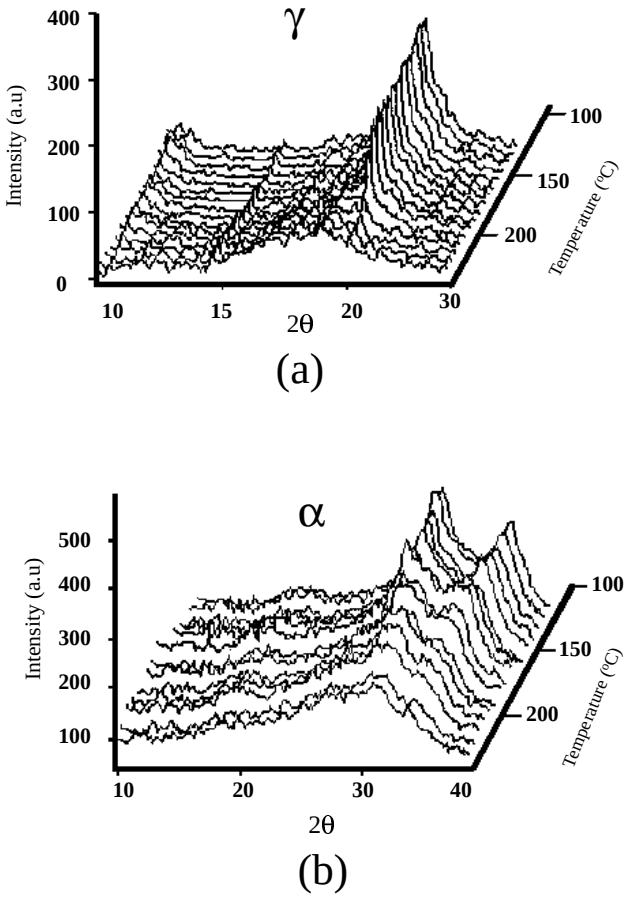

Fig. 11. WAXD patterns under cooling after shearing: (a) NCH5; (b) Nylon 6.

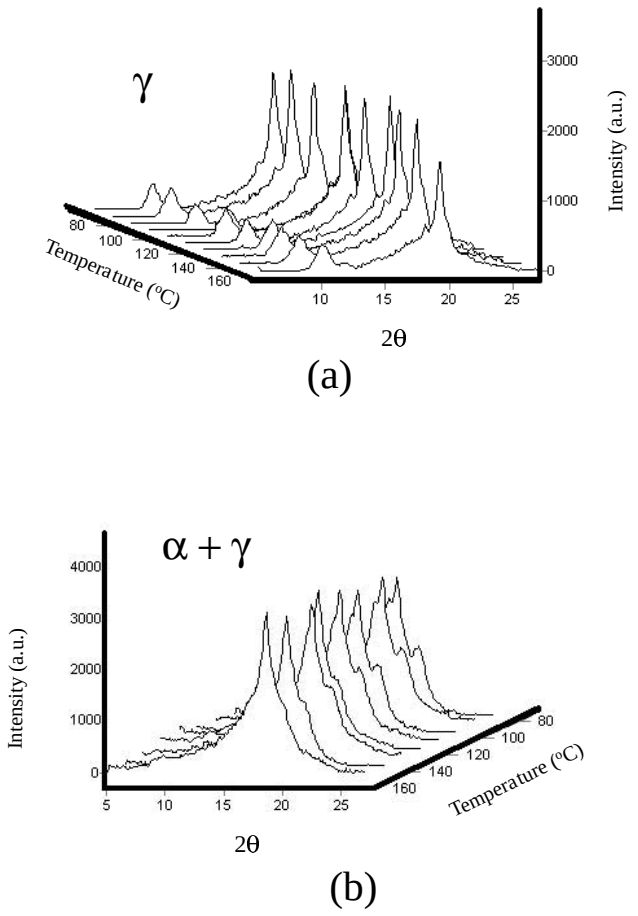

Fig. 12. WAXD patterns of (a) NCH5 and (b) Nylon 6 during quiescent crystallization.

Nylon 6 both α and γ crystal habits are formed during quiescent crystallization. However, only α-form is seen in the shear experiment of Nylon 6 (Fig. 11b). This indicates that shear hinders the formation of the γ-form or it favors the formation of the α-form. In contrast, the NCH_5 hybrid can crystallize into the γ-form when shear is applied or not. Therefore, it can be concluded that the shear process does not affect the induction of the γ-form, which is mainly attributed to the presence of exfoliated clay. As for the imposed thermal condition, it was the same in both cases.

4. Conclusions

The orientation behavior in nanocomposites based on Nylon 6 and montmorillonite was studied by in situ synchrotron X-ray methods. We found that the system can be oriented under relatively low shear fields and temperatures immediately above the experimental melting temperature. The orientation of the polymer and clay composite manifests itself as an equatorial through-view SAXS pattern, depending on the clay content and shear time. The orientation induced by shear was found to increase with shear time and remain stable for relatively long times in the molten state. Dynamic non-isothermal crystallization is an effective means to preserve the orientation. WAXD patterns obtained from quiescent and shear non-isothermal crystallization experiments indicated that the presence of exfoliated clay is the primary reason to induce the oriented γ-form under shear.

Acknowledgements

F.J. Medellin-Rodriguez would like to thank the National Research Council of Science and Technology (CONACyT) of Mexico for partial support during his sabbatical year at SUNY, Stony Brook. The financial support of this work provided by the National Science Foundation of the USA (DMR-0098104) and the US Army Research Office (DAAD190010419) is gratefully acknowledged.

References

[1] Okada A, Kawasumi M, Usuki A, Kojima Y, Kurauchi T, Kamigaito O. Mater Res Soc Symp Proc 1990;171:45.
[2] Usuki A, Kojima Y, Kawasumi M, Okada A, Kurauchi T, Kamigaito O, Deguchi R. Polym Prepr Jpn 1990;39(8):2427.

[3] Kojima Y, Okada A, Usuki A, Kawasumi M, Kurauchi T, Kamigaito O, Deguchi R. Polym Prepr Jpn 1990;39(8):2430.
[4] Kojima Y, Usuki A, Kawasumi M, Okada A, Fukushima Y, Kurauchi T, Kamigaito O. J Mater Res 1993;8:1185.
[5] Ke Y, Long C, Qi Z. J Appl Polym Sci 1999;71:1139.
[6] Messersmith PB, Giannelis EP. J Polym Sci, Part A: Polym Chem 1995;33:1047.
[7] Vaia RA, Price G, Ruth PN, Nguyen HT, Lichtenhan J. Appl Clay Sci 1999;15:67.
[8] Kojima Y, Usuki A, Kawasumi M, Okada A, Kurauchi T, Kamigaito O. J Appl Polym Sci 1993;49:1259.
[9] Krishnamoorti R, Giannelis EP. Macromolecules 1997;30:4097.
[10] Kojima Y, Usuki A, Kawasumi M, Okada A, Kurauchi T, Kamigaito O, Kaji K. J Polym Sci B: Polym Phys 1994;32:625.
[11] Kojima Y, Usuki A, Kawasumi M, Okada A, Kurauchi T, Kamigaito O, Kaji K. J Polym Sci B: Polym Phys 1995;33:1039.
[12] Brill R. Z Physik Chem B 1943;53:61.
[13] Holmes R, Bunn DW, Smith DL. J Polym Sci 1955;17:619.
[14] Arimoto H, Ishibashi M, Hirai M, Chatani Y. J Polym Sci 1965;A3:317.
[15] Samon JM, Schultz JM, Wu J, Hsiao B, Yeh F, Kolb R. J Polym Sci, Part B: Polym Phys 1999;37:1277.
[16] Kojima Y, Usuki A, Kawasumi M, Okada A, Kurauchi T, Kamigatio O. J Polym Sci A: Polym Chem 1993;31:983.
[17] Usuki A, Kojima Y, Kawasumi M, Okada A, Fukushima Y, Kurauchi T, Kamigatio O. J Mater Res 1993;8:1179.
[18] Buchner S, Wiswe D, Zachmann HG. Polymer 1989;30:480.
[19] Kyotani M, Mitsuashi S. J Polym Sci A 1972;2(10):1497–508.
[20] Gurato G, Fichera A, Grandi FZ, Zanneti R, Canal P. Die Makromol Chem 1974;175:953–75.
[21] Kojima Y, Matzuoka T, Takahashi H, Kuaruchi T. J Appl Polym Sci 1994;51:683.
[22] Statton WO. J Polym Sci 1962;58:205.
[23] Alexander LE. X-ray diffraction methods in polymer science. New York: Wiley, 1969.